Exploration of the Dual Active Full Bridge DC-DC Converter using Optimization Technique

G. Jhansi Rani[1], E. Vidya Sagar[2]

[1]Research Scholar, EEE Department, OUCE, Osmania University, Hyderabad, India
[2]Professor, EEE Department, OUCE, Osmania University, Hyderabad, India

Abstract- This paper presents an exploration of the Dual Active Full Bridge (DAFB) converter utilizing optimization techniques to improve its performance. The DAFB DC-DC converter is gaining prominence in power electronic applications due to its ability to efficiently manage power levels while maintaining compact size and enhanced control capabilities. The use of a trial and error method to select Proportional Integral (PI) gain values in controllers does not result in accurate values that can be used for tuning the controller. To circumvent this, it is easier to go with optimization techniques because these techniques perform the search operations to fit suitable values for the gain parameters. Hence, Cuttlefish Optimization technique is used in this paper to select optimum values of PI gains. This results in a reduction in the amount of time necessary to obtain the gain parameters.

Key Words: DAFB, Proportional Integral, Cuttlefish Optimization (CFO), PV system, Voltage Controller.

I. INTRODUCTION

In terms of potential solutions for achieving sustainable development, the forms of renewable energy that hold the most promise are solar [1] and wind power. The demand for environmentally friendly forms of electricity has never been higher. In order to satisfy this demand, electric power systems will need to mature to the point where they can accommodate the incorporation of renewable energy sources like wind and solar, and they will also need to be able to provide high capacity battery backup in the event of a blackout. In recent years, there has been an increasing demand for the integration of renewable energy sources (RES) into conventional grids. The development of power electronic converters and the advancement of power semiconductor devices have made it possible for renewable energy sources to be directly integrated into the grid that is already in place [2]. This can be accomplished through the utilisation of a variety of power converter topologies. In order for renewable energy sources (RES) to function at their maximum power point, the interface is provided by DC to DC [3-4] converters. On the other hand, DC to AC inverters are utilised as the interface to the conventional 50Hz grid. When it comes to controlling any DC to DC or DC to AC converter, the most common method is a dual loop control, which consists of an outer voltage loop and an inner current loop. This is because it restricts the amount of current that can flow through the converter. When it comes to the Dual Active Bridge Converter, the inner current control is implemented through the utilisation of half cycle moving window averaging on the high frequency transformer current. It is the outer voltage loop that provides the reference current that is desired. On the secondary side of the DAB converter, the duty cycle mode of control suggests an alternative switching strategy that can be implemented. Half of the time, the primary side is switched to the secondary side. Through the utilisation of duty cycle modulation, the secondary side switches are set to operate independently. The grid connected PV system is addressed in [5-7].

II. METHODOLOGY

Fig. 1 is an illustration of the configuration that has been suggested. Figures 2 and 3 depict the control circuit that is utilised for bridge 1 (the primary side converter) and bridge 2 (the secondary side converter), respectively. By integrating DAFB [8], Solar photovoltaic are utilised for the purpose of charging the batteries. The solar model has three components: 1) a light-induced current source known as I_{LG}; 2) a P-N junction diode that is shunted; and 3) a shunt branch resistance known as R_{sh} that is

responsible for the leakage currents caused by the impurities in the P-N junction. The value of this resistance must be as high as possible. In the best possible scenario, R_{sh} approaches infinity. 4) A resistance, R_{se}, that is connected in series and reflects the total ohmic resistance spread in the semiconductor as well as the resistance of the metal that interacted with it. In a perfect scenario, the value of the series resistance should correspond to zero. I_{dll} is the value of the current that is flowing through a shunt branch P-N junction diode.

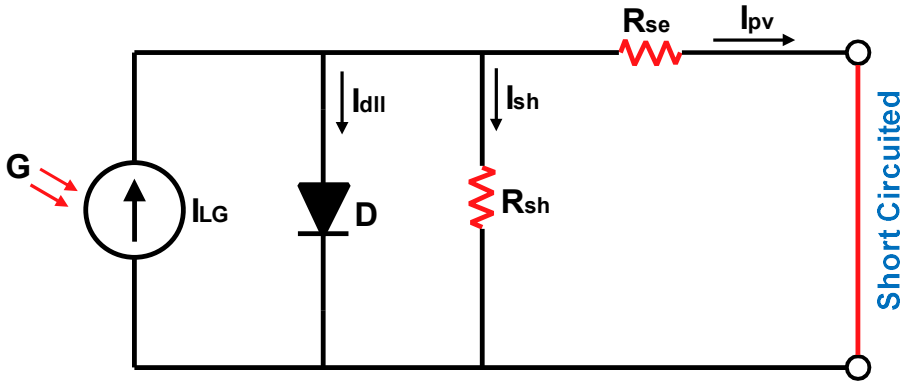

Fig. 1: Equivalent circuit under short-circuited

From Fig.1, the I_{pv} is expressed as,

$$I_{pv} = I_{LG} - I_{dll} - I_{sh} \quad (1)$$

The voltage across them governs the current flowing through the elements,

$$V_{dp} = V_{pv} + I_{pv}R_{se} \quad (2)$$

Where, V_{pv} = Output voltage of PV cell/array in volts, I_{pv} = Output current of PV cell/array and V_{dp} = Voltage drop across diode.

Generally, diode current describes as follows,

$$I_{dll} = I_{ds}\left[e^{\frac{QV_{pv}}{nKT}} - 1\right] \quad (3)$$

Where, Q = electron charge = 1.6022 x 10^{-19} C, K = Boltzmann's constant = 1.3807 x 10^{-23} JK^{-1}, n = Quality factor of diode, T = Working temperature of cell's in kelvin, I_{ds} = Saturation current.

It includes the effect of series resistance, then diode current becomes,

$$I_{dll} = I_{ds}\left[e^{A(V_{pv}+I_{pv}R_{se})} - 1\right] \quad (4)$$

Where,

A = Constant = $\frac{Q}{nKT}$

The current in shunt branch resistance, I_{sh}, as per OHM's law is,

$$I_{sh} = \frac{V_{dp}}{R_{sh}} = \frac{V_{pv}+I_{pv}R_{se}}{R_{sh}} \quad (5)$$

Therefore, the output current I_{pv} is given by substituting Eqns.(4), and (5) in (1)

$$I_{pv} = I_{LG} - I_{ds}\left[e^{A(V_{pv}+I_{pv}R_{se})} - 1\right] - \frac{V_{pv}+I_{pv}R_{se}}{R_{sh}} \quad (6)$$

Eqn. (6) is valid for a single cell, But a PV array contains a matrix of several cells in practice. By seeing the array of N_s number of cells for one module or one panel Eqn.(6) can be written as

$$I_{pv} = I_{LG} - I_{ds}\left[e^{A\left(\frac{V_{pv}+I_{pv}R_{se}}{N_s}\right)} - 1\right] - \frac{V_{pv}+I_{pv}R_{se}}{R_{sh}} \quad (7)$$

To meet the high voltage demand number of PV cells are added in series, N_{sl}, and to meet the high current demand number of cells are connected in parallel, N_{ll}, as shown in Fig.9.

So, Eqn. (7) can be written as,

$$I_{pv} = N_{ll}I_{LG} - N_{ll}I_{ds}\left[e^{A\left(\frac{V_{pv}}{N_sN_{sl}}+\frac{I_{pv}R_{se}}{N_sN_{ll}}\right)} - 1\right] - \left[\frac{N_{ll}^2V_{pv}+N_{ll}N_{sl}(I_{pv}R_{se})}{N_{ll}N_{sl}R_{sh}}\right] \quad (8)$$

The light-induced current produced by the PV cell depends on solar irradiation and by the temperature according to the following equation

$$I_{LG} = [I_{sc} + k_i(T - T_*)]\frac{G}{G^*} \quad (9)$$

Here, I_{sc} (A) is the short circuit current, generally, at 25^{0}C and 1000 W/m^2, k_i is short circuit current temperature coefficient. T (K) and T_* are actual or operating temperatures, and reference temperature (25^{0}C or 298K), G (W/m^2) is the solar irradiation or insolation, and G^* is the reference irradiation (1000 W/m^2).

The diode saturation current I_{ds} is expressed as:

$$I_{ds} = I_{rs}\left[\frac{T}{T_*}\right]^3 exp\left[\frac{QE_{gb}}{nK}\left(\frac{1}{T}-\frac{1}{T_*}\right)\right] \quad (10)$$

Where, E_{gb} is the semiconductor band gap energy typically ≈1.12eV for polycrystalline Si at 25^{0}C, and I_{rs} is the reverse saturation current at the reference temperature.

Therefore, reverse saturation current is,

$$I_{rs} = \frac{I_{sc}}{exp\left[\frac{A.V_{oc}}{N_s}\right]-1} \quad (11)$$

Where, V_{oc} is the open circuit voltage, the following expressions will now be used to enhance the PV model.

$$I_{ds} = \frac{I_{sc}+k_i\Delta_T}{exp\left[\frac{A(V_{oc}+k_v\Delta_T)}{N_s}\right]-1} \quad (12)$$

Where, $\Delta_T = T - T_*$, k_v = Voltage temperature coefficient

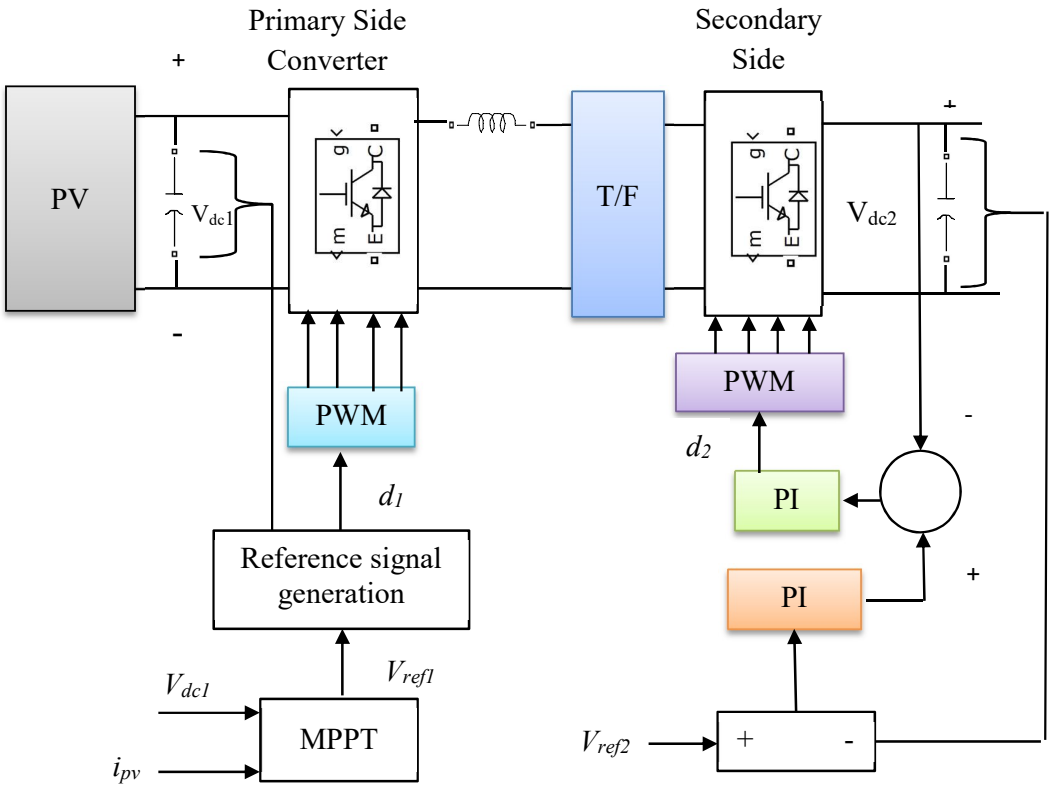

Fig.2: Block diagram used for simulation

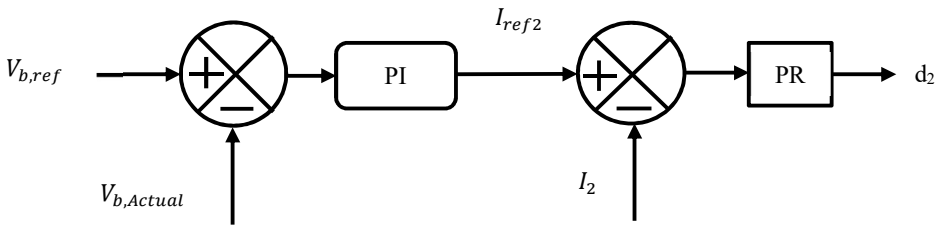

Fig.3: Control block diagram for converter 2

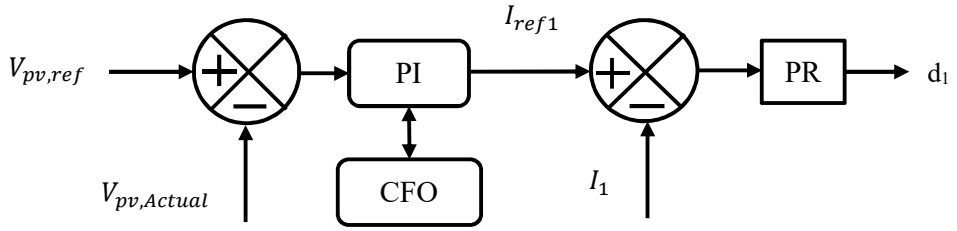

Fig.4: Control block diagram for converter 1

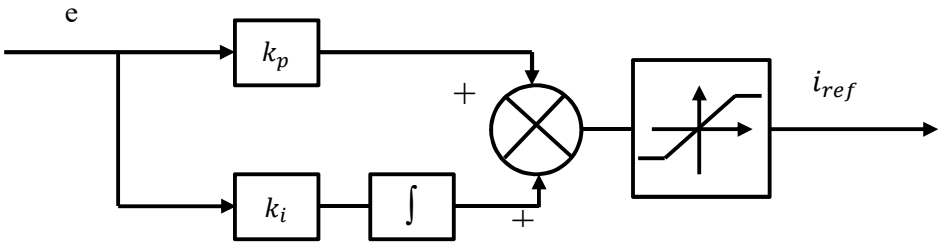

Fig.5: Block diagram of PI controller

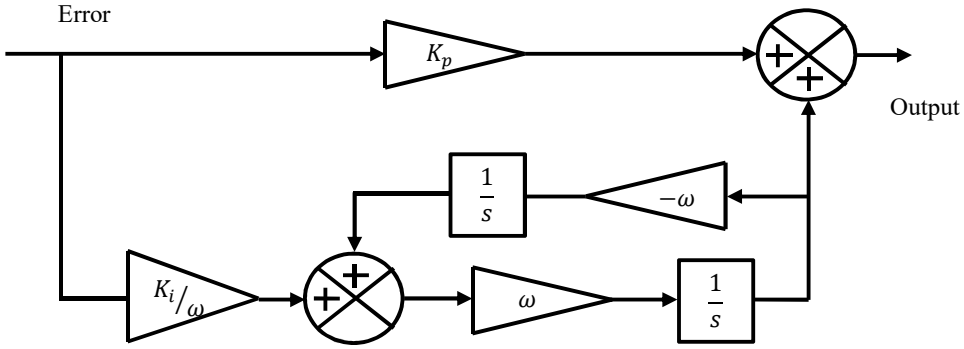

Fig. 6: Block diagram of PR current regulator

The block diagram is used in this work is illustrated in Fig.2.The control block diagram for converter2 and converter1 is presented in Fig.3 and Fig.4 respectively. Fig.5 illustrates a block diagram of a conformist PI regulator [9-15]. The schematic block diagram of resonant current regulator is illustrated in Fig.6. Transfer function of ideal Proportional and Resonant (PR) controller: $G_{PR}(s) = k_p + \frac{k_i s}{s^2+\omega^2}$. Where, ω stands the system angular frequency, k_p and k_i are the proportional constant and integral constant respectively.

The generalized PI controller expressed as follows,

$$v(t) = k_p e(t) + k_i \int e(t)\, dt \tag{1.16}$$

Where, $v(t)$ is linear control signaling output and $e(t)$ is error signal generated by comparing the actual signal with reference signal.

The minimum values of parameters for PI technique can be determined using Eqn. (1.17).

$$\left.\begin{matrix} k_p \geq 2C\xi\omega \\ k_i \geq C\omega \end{matrix}\right| \tag{1.17}$$

Where, *k_p, ki, C, ξ and ω* are proportional constant, integral constant, dc-link capacitance, damping coefficient (0.707) and system angular frequency respectively.

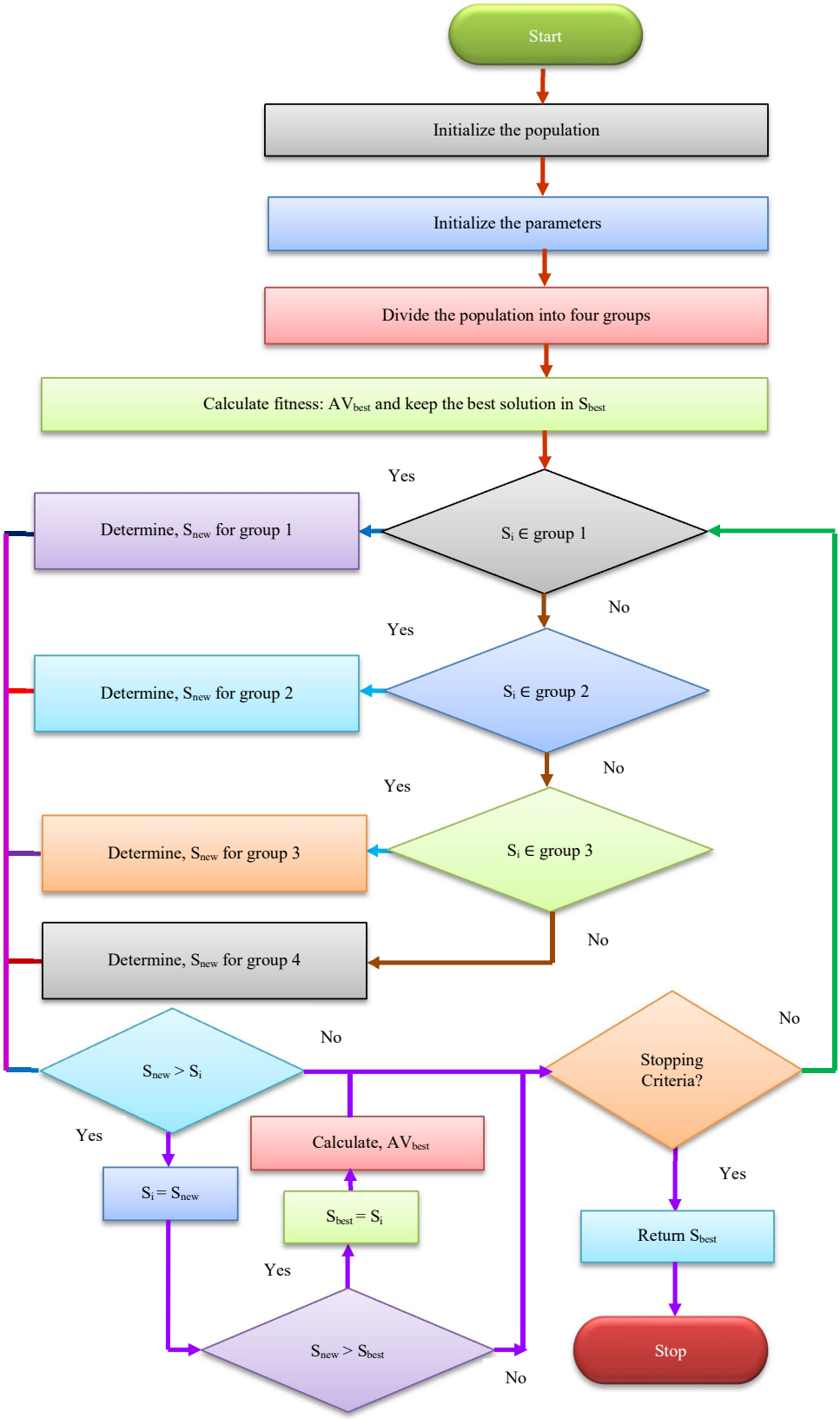

Fig.7: Flowchart of CFO algorithm

For the purpose of operating the DAFB converter, a number of different modulation techniques were proposed. The conventional phase-shift modulation, also known as the single phase-

shift modulation (SPS), is the most straightforward and straightforward method to implement. This method allows for the power to be controlled by a straightforward PI-based controller. The incremental conductance is used for thee extraction of the maximum power [16-22]. The complete steps for CFO algorithm [23-24] are framed in flowchart as presented in Fig.7.

III. SIMULATION RESULT AND DISCUSSION

The block diagram shown in Fig.2 is simulated and the corresponding results are presented in this section. The simulation parameters are listed in Table I and Table II. The simulation results are presented for two cases including standard atmospheric conditions (SAC) and change of atmospheric conditions (CAC).

Table I: Controller parameters

CFO tuned PI	K_p=81.472368639317890, K_i=0.090579193707562
Voltage Controller 2	K_p=0.01, K_i=0.0001
Current Controller 1	K_p=0.01, K_i=0.0001
Current Controller 2	K_p=-0.01, K_i=0.00001

Table II: Parameters used for simulation

Parameter	Value
Input Voltage	255 V
Battery SoC	50%
Battery type	Lithium ion
Capacitor	3300 μF
Transformer	1:1 single phase transformer, 250 V, 50 Hz
Inductor	0.5 mH
PV parameters	
V_{oc}	37.5 V
I_{sc}	3.3 A
R_{se}	0.01 Ω
R_{sh}	200 Ω
N_{series}	7
$N_{parallel}$	7
PV reference Voltage	263 V

Case 1: Standard atmospheric condition

The simulated results for the case 1 are illustrated in Fig.8 with incremental conductance MPPT controller and CFO tuned PI controller. The proposed configuration is simulated in both charging and discharging conditions. PV is integrated during charging conditions and disconnected in discharging mode. The battery current is circulated through LC filter in discharging condition. The state of charge (SOC) is considered as 50% for the simulation illustration. The PV voltage using MPPT controller is controlled effectively during change of atmospheric condition from t=3s to t=6s.

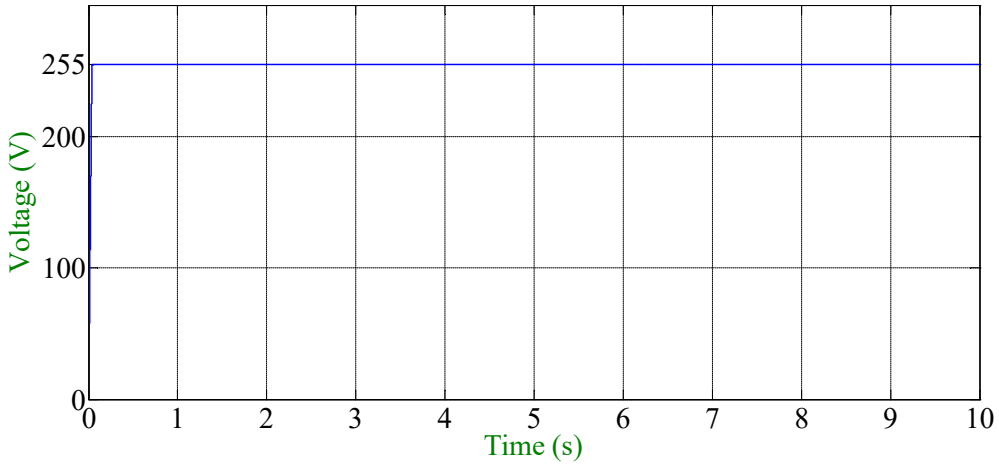

(a) PV Voltage

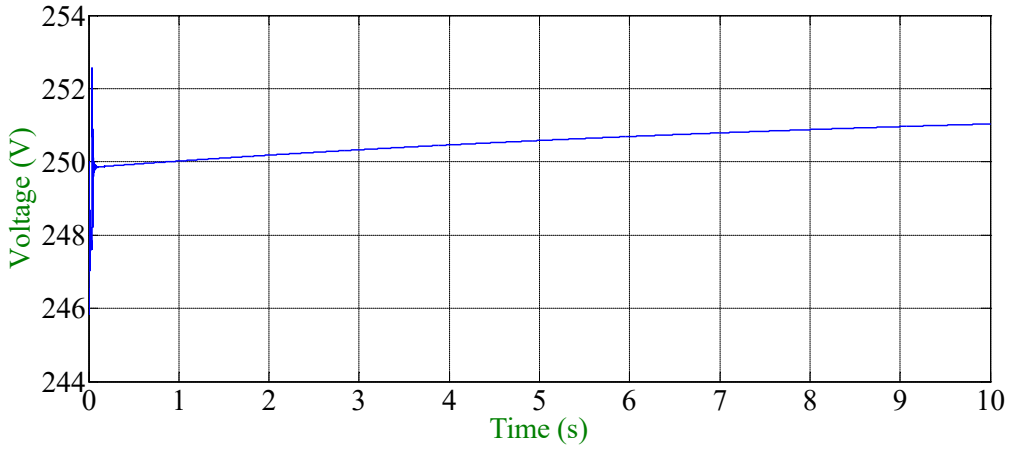

(b) Battery Voltage

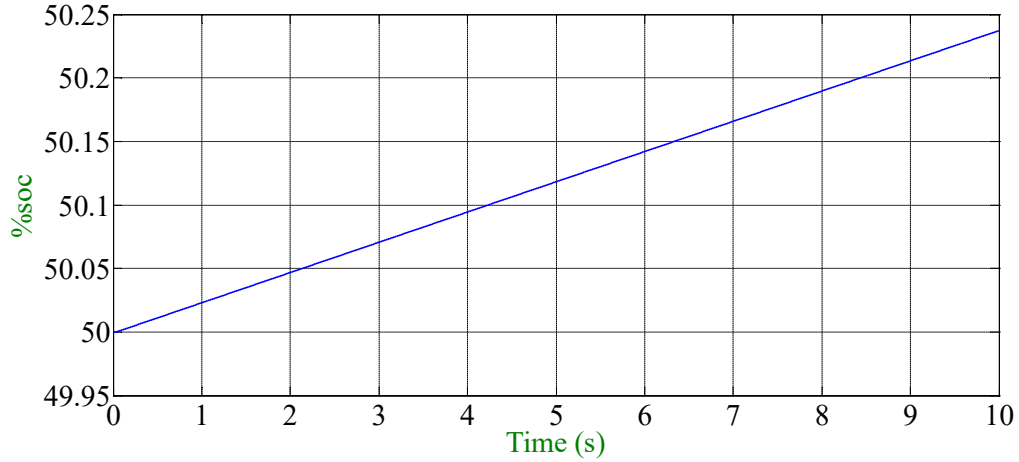

Fig.8: Response curves under charging mode using PI- CFO and PI

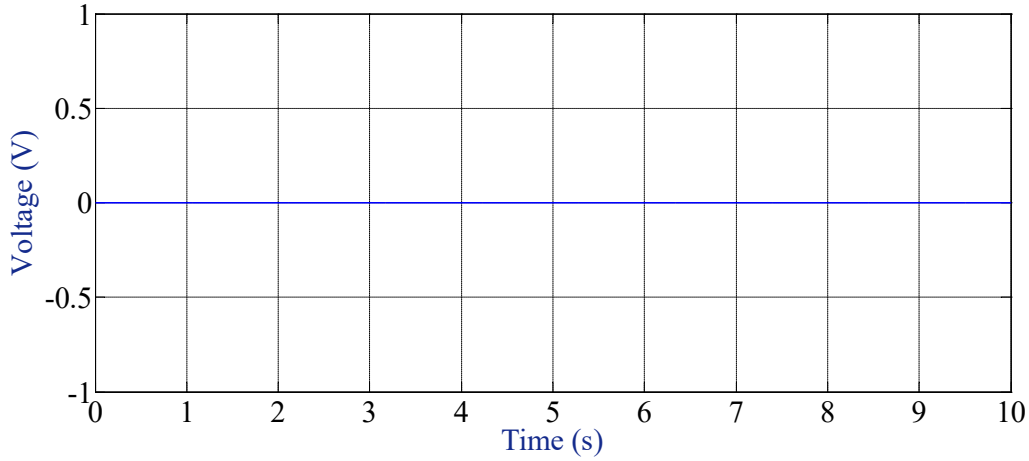

(a) PV Voltage

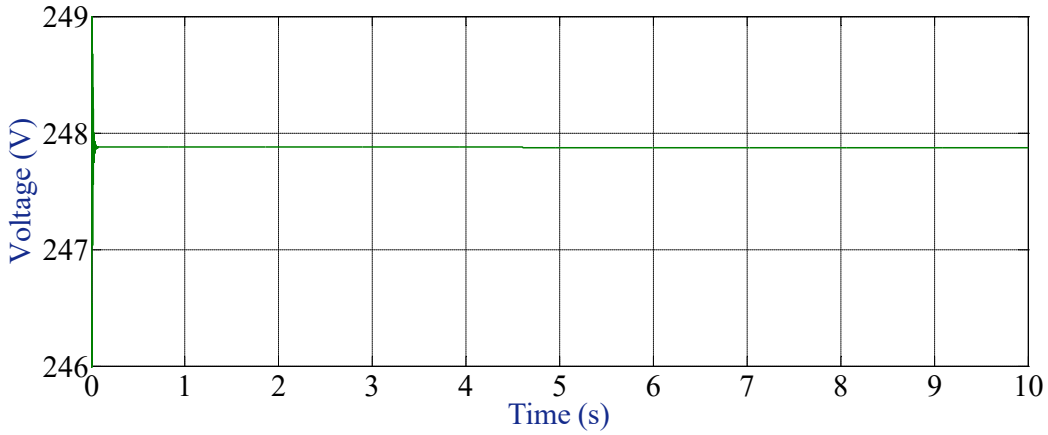

(b) Battery Voltage

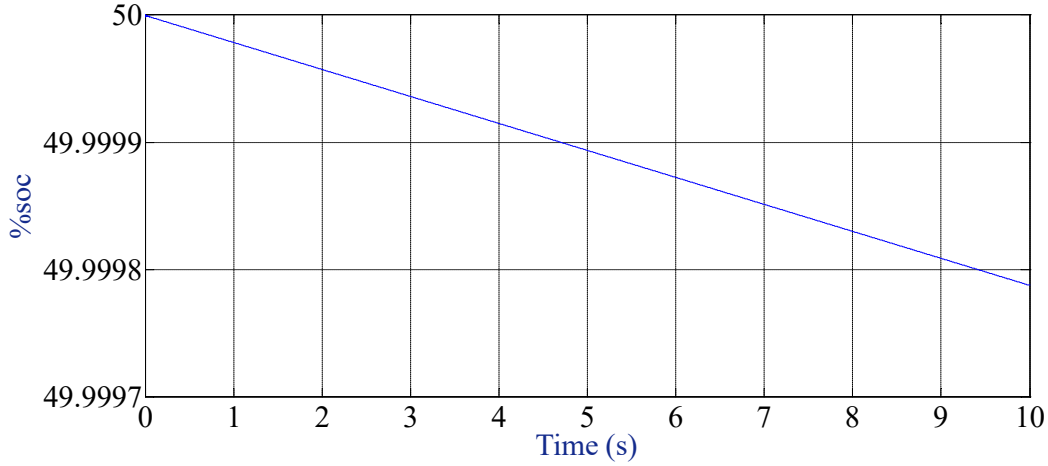

(c) SOC

Fig.9: Response curves under discharging mode using PI-CFO and PI

The PV integrated battery is simulated under constant irradiation and is illustrated in Fig.8. The PV voltage is tracking the reference with a value of 250V and is illustrated Fig.8 (a). The battery charging status is depicted in Fig.8 (b). The % soc is presented in Fig.8 (c). The battery discharging status is depicted in Fig.9 (b). The % soc is presented in Fig.9 (c).

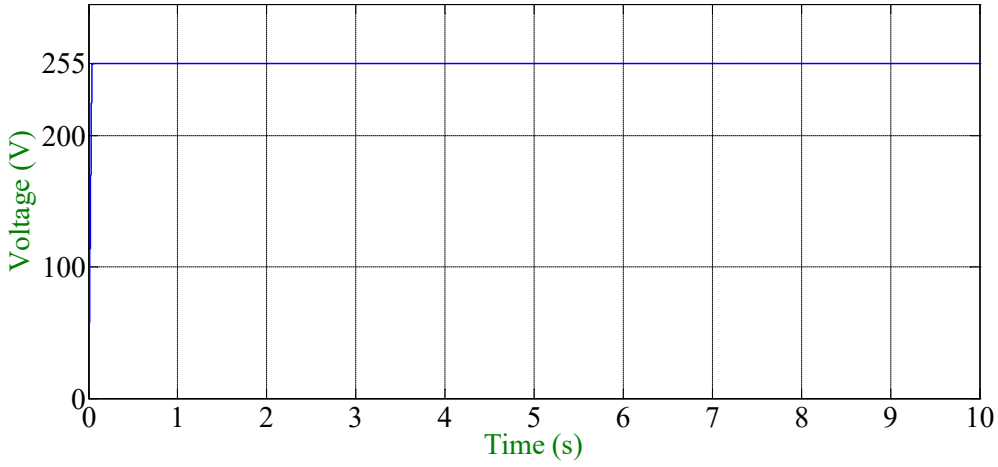

(a) PV Voltage

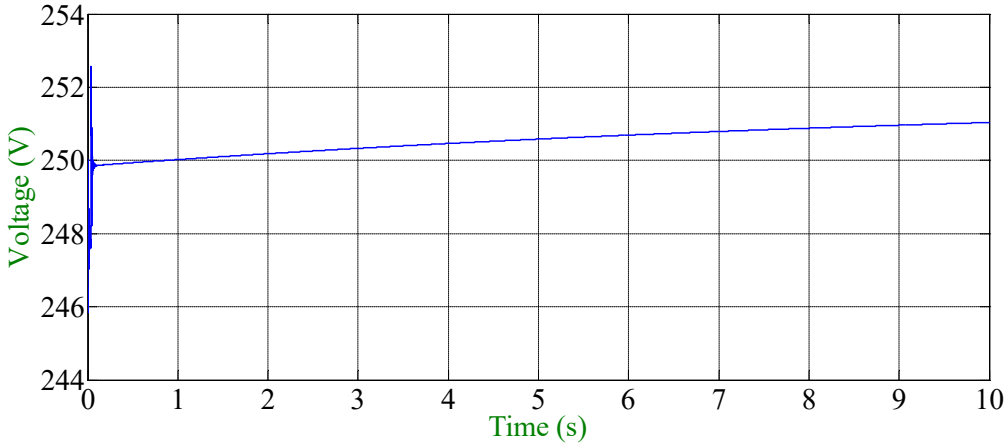

(b) Battery Voltage

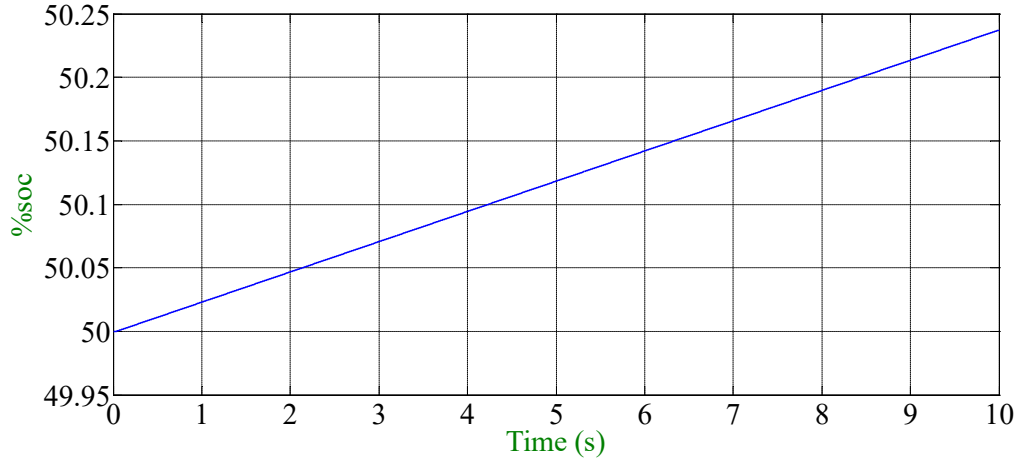

Fig.10: Response curves under charging mode using PI-CFO and PR

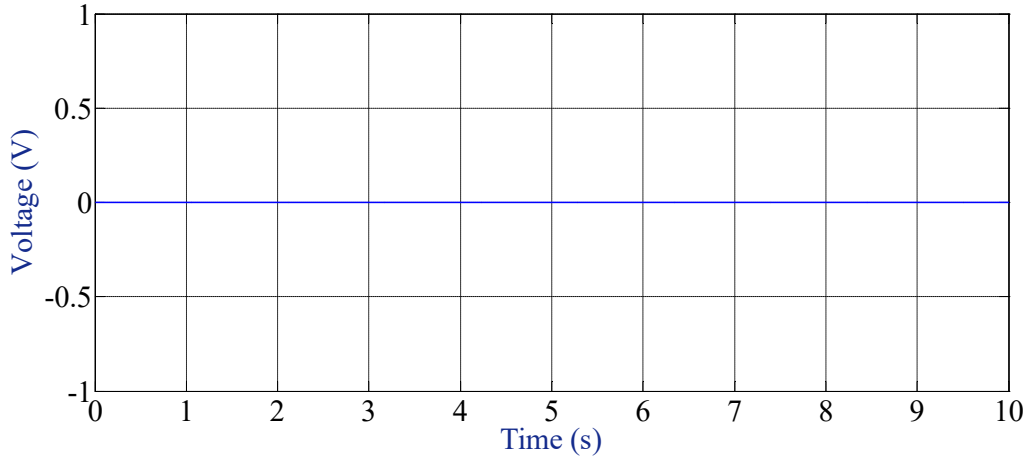

(a) PV Voltage

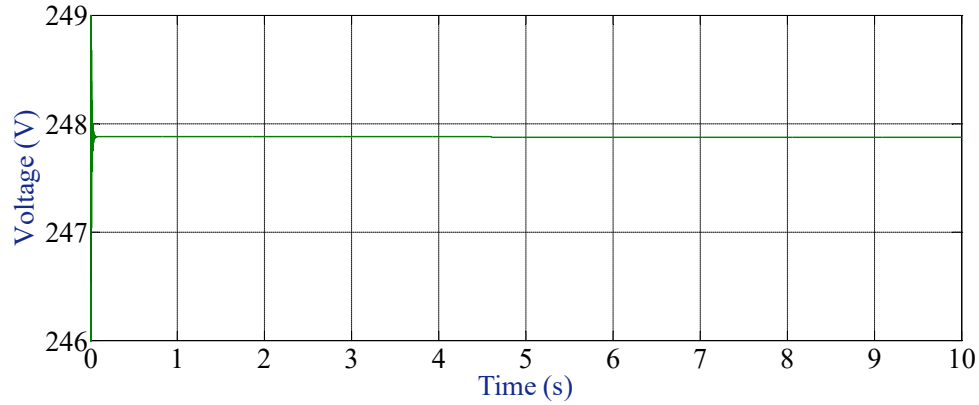

(b) Battery Voltage

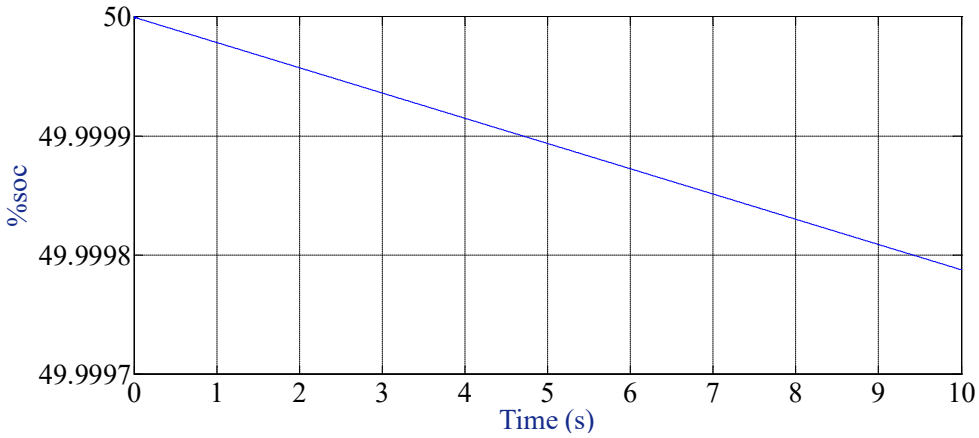

(c) SOC

Fig.11: Response curves under discharging mode using PI- CFO and PR

The PV integrated battery is simulated under constant irradiation and is illustrated in Fig.2. The PV voltage is tracking the reference with a value of 250V and is illustrated Fig.10 (a). The battery charging status is depicted in Fig.10 (b). The % soc is presented in Fig.10 (c). The battery discharging status is depicted in Fig.5.11 (b). The % soc is presented in Fig.5.11 (c).

Case 2: Change of atmospheric condition

The PV integrated battery is simulated under variable irradiation and is illustrated in Fig.12. The PV voltage is tracking the reference with a value of 250V and is illustrated Fig.12 (a). The battery charging status is depicted in Fig.12 (b). The % soc is presented in Fig.12 (c). The battery discharging status is depicted in Fig.13 (b). The % soc is presented in Fig.13 (c).

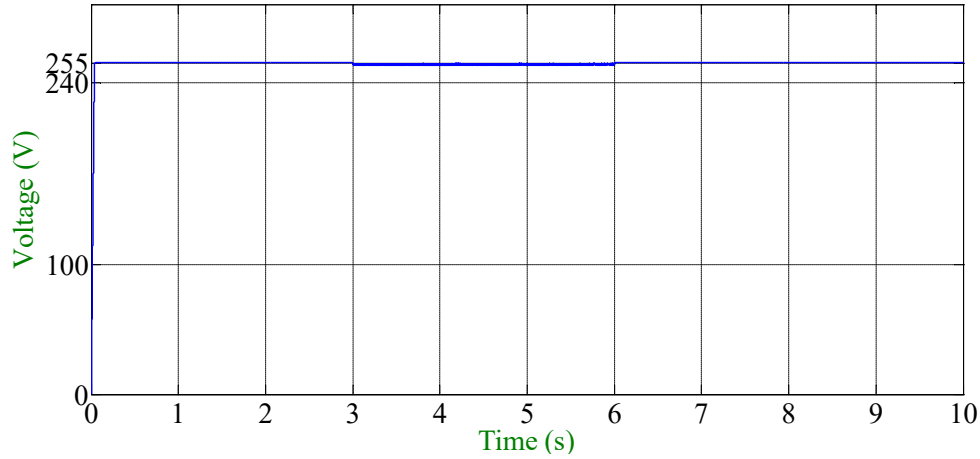

(a) PV Voltage

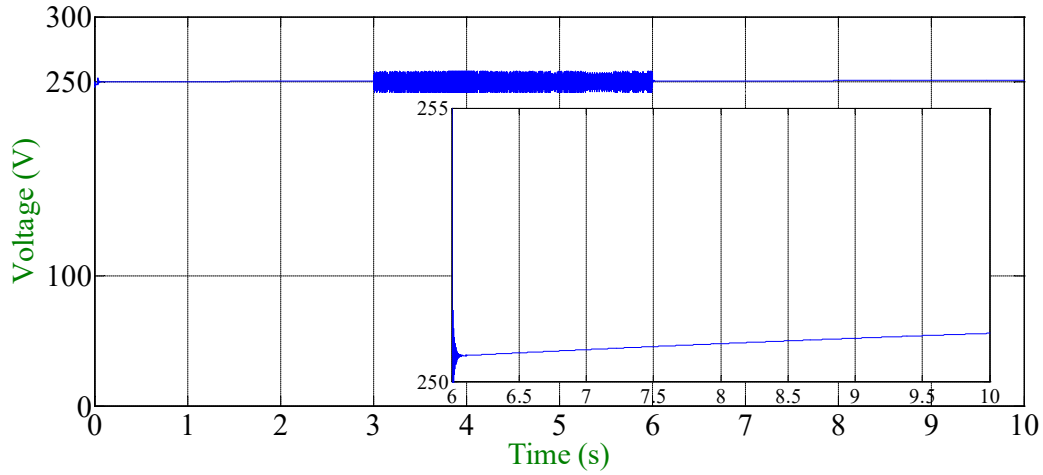

(b) Battery Voltage

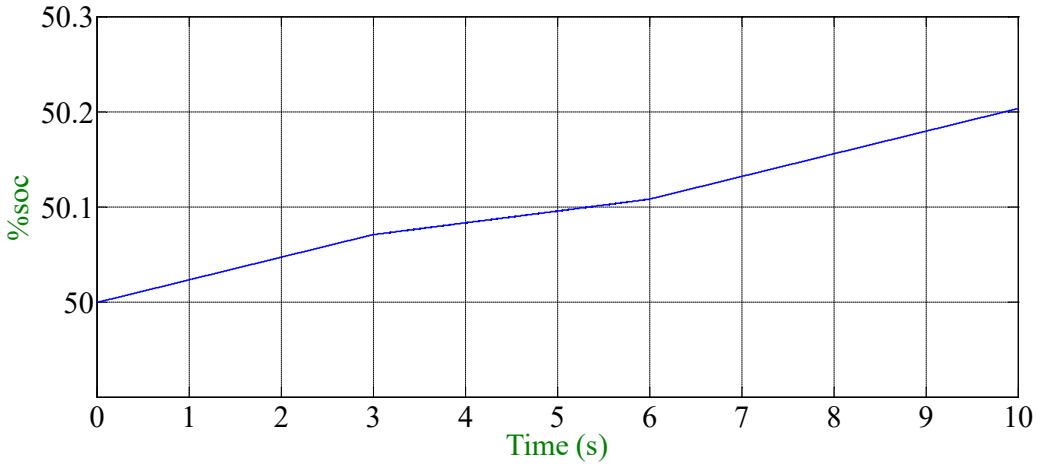

(c) SOC

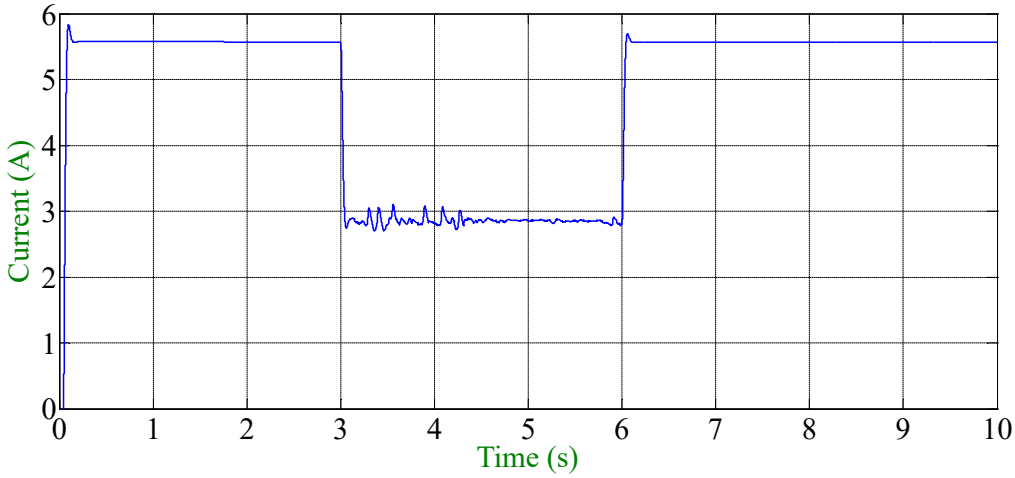

(d) Battery Current

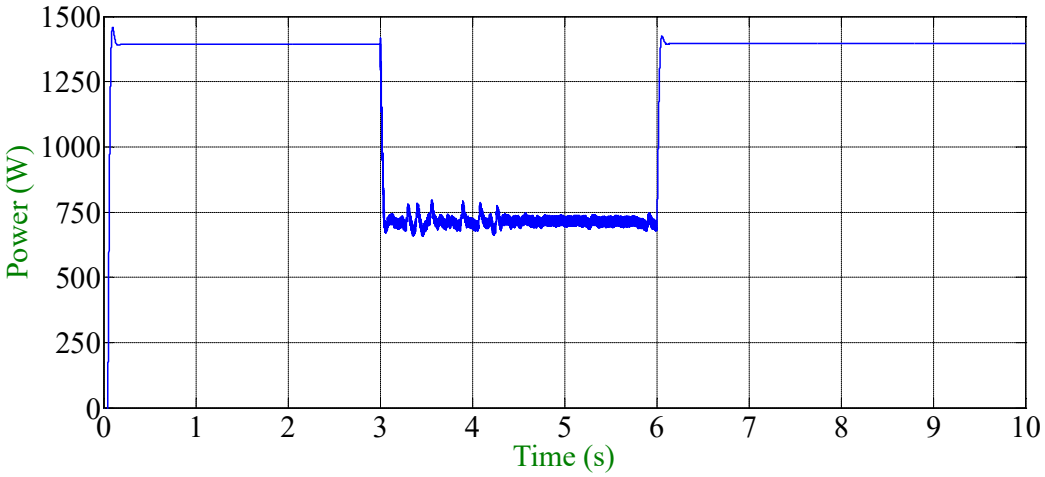

(e) Battery Power

Fig.5.12: Response curves under charging mode using PI-CFO and PI

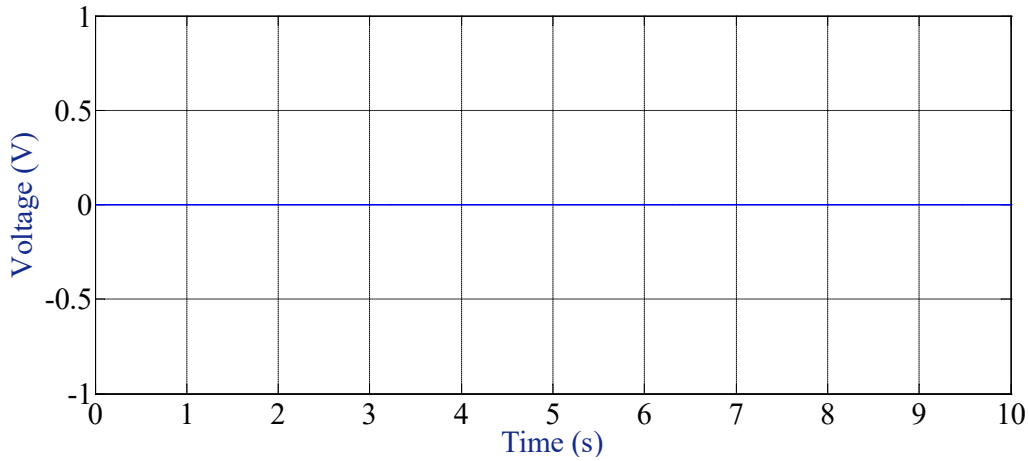

(a) PV Voltage

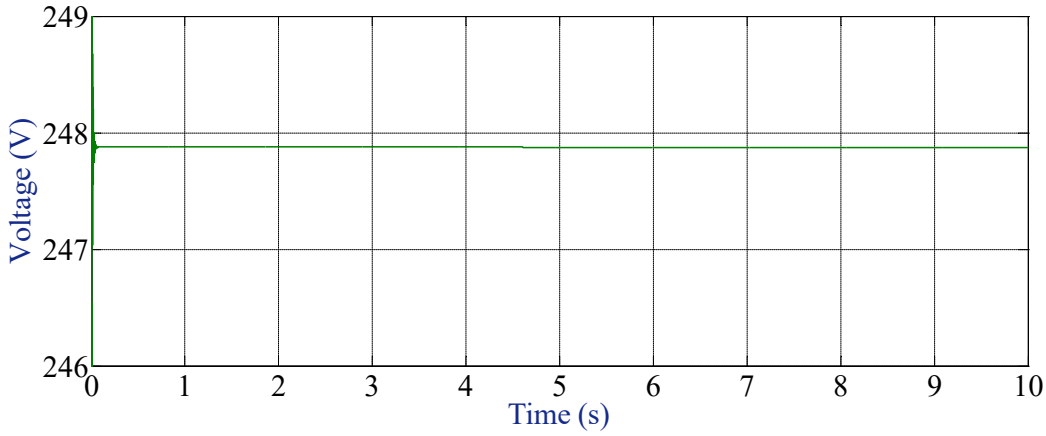

(b) Battery Voltage

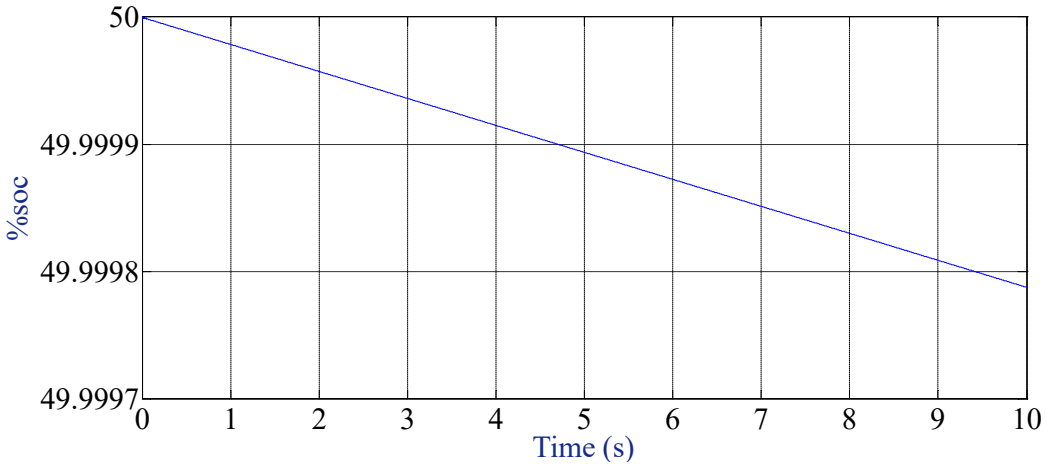

(c) SOC

Fig.5.13: Response curves under discharging mode using PI-CFO

IV. CONCLUSION

The concept of cuttlefish optimization for PV integrated DAFB is presented. The simulation results are presented for proposed configuration in two cases such as for constant and variable irradiance. The performance of proposed configuration is performed well in both conditions including SAC and CAC using CFO. The SOC is presented in both charging and discharging conditions for 50% SOC. The battery voltage is exactly followed the %SOC. The charging mode defined in this work is the PV integrated DAFB. In discharging mode, the PV is turned off so that the battery starts discharging.

The utilization of the Cuttlefish optimization algorithm for the DC link voltage control of PV integrated Dual Active Full Bridge (DAFB) converters represents a promising and innovative approach. The Cuttlefish optimization algorithm optimizes the DC link voltage control strategy, resulting in improved energy conversion within the PV-DAFB system. This leads to more efficient use of the harvested solar energy. By continuously adapting the DC link voltage to maintain the PV panel at its maximum power point (MPPT) and ensuring stable output voltage, the algorithm guarantees the optimal operation of the converter. The algorithm's adaptability and optimization capabilities make it robust and reliable in varying environmental conditions and load requirements, enhancing the overall system's resilience and stability.

The utilization of advanced optimization algorithms like Cuttlefish represents an innovative approach to control systems, demonstrating the potential for ongoing technological advancements in the field of renewable energy (RE) integration.

REFERENCES

[1]. M. M. Nour, A. A. Helal, M. M. El-Saadawi, and A. Y. Hatata, “A control scheme for voltage unbalance mitigation in distribution network with rooftop PV systems based on distributed batteries,” *International Journal of Electrical Power & Energy Systems*, Jan. 01, 2021. https://www.sciencedirect.com/science/article/abs/pii/S014206152031293X

[2]. K. Bhandari, I. V. Kumar and K. Srinivas, "Cuttlefish Algorithm-Based Multilevel 3-D Otsu Function for Color Image Segmentation," in IEEE Transactions on Instrumentation and Measurement, vol. 69, no. 5, pp. 1871-1880, May 2020, doi: 10.1109/TIM.2019.2922516.

[3]. S. Meenakshi, K. Rajambal, C. Chellamuthu, and S. Elangovan, “Intelligent controller for a stand-alone hybrid generation system,” 2006 IEEE Power India Conference, 2006, Published, doi: 10.1109/poweri.2006.1632599.

[4]. S. Dutta and S. Bhattacharya, "Predictive current mode control of single phase dual active bridge DC to DC converter," 2013 IEEE Energy Conversion Congress and Exposition, Denver, CO, USA, 2013, pp. 5526-5533, doi: 10.1109/ECCE.2013.6647451.

[5]. M. A. Mahmud, H. R. Pota, M. J. Hossain and N. K. Roy, Robust partial feedback linearizing stabilization scheme for three-phase grid-connected photovoltaic systems, IEEE Journal of Photovoltaic, vol. 4, no. 1, pp. 564–571, pp.423-431, January 2014.

[6]. M. A. Mahmud, H. R. Pota, and M. J. Hossain, “Dynamic stability of three-phase grid-connected photovoltaic system using zero dynamic design approach,” IEEE J. Photovoltaic, vol. 2, no. 4, pp. 564–571, Oct.2012.

[7]. M. A. Mahmud; M. J. Hossain; H. R. Pota; N. K. Roy, Robust Nonlinear Controller Design for Three-Phase Grid-Connected Photovoltaic Systems Under Structured Uncertainties, IEEE Transactions on Power Delivery, vol. 29, no. 3,pp. 1221 - 1230, June 2014.
[8]. Y. Nagaraja, T. Devaraju, A. M. Sankar, and V. Narasimhulu, "PV and Wind Energy Conversion Exploration based on Grid Integrated Hybrid Generation Using the Cuttlefish Algorithm," Engineering, Technology & Applied Science Research, vol. 12, no. 6, pp. 9670–9675, Dec. 2022.
[9]. V. Narasimhulu and K. Jithendra Gowd, "Performance Analysis of Single-Stage PV Connected Three-Phase Grid System Under Steady State and Dynamic Conditions," in Cybernetics, Cognition and Machine Learning Applications, Singapore, 2021, pp. 39–46, https://doi.org/10.1007/978-981-33-6691-6_5.
[10]. G. Jhansi Rani, P. Srinivas, performance exploration of single phase DAB DC-DC converter under load variation, International Research Journal of Engineering and Technology, vol. 10, no. 4, pp.1029-1035, Apr 2023.
[11]. Pablo F. S. Costa, Pedro H. B. Löbler, Leandro Roggia, and Luciano Schuch. Modeling and Control of DAB Converter Applied to Batteries Charging, IEEE Transactions on Energy Conversion, Vol. 37, No. 1, March 2022.
[12]. V. Narasimhulu, "Simulation Analysis of Switch Controlled power filters for harmonic reduction", an International Journal of Applied Engineering Research, 2016, Vol.: 11, Issue: 11, pp. 7597- 7602.
[13]. Haochen Shi, et.al, "Minimum-Reactive-Power Scheme of Dual-Active-Bridge DC–DC Converter With Three-Level Modulated Phase-Shift Control", IEEE Transactions on Industry Applications, Vol. 53, No. 6, pp.5573-5586, November/December-2017.
[14]. Jianqiang Liu, et al., "Voltage Balance Control Based on Dual Active Bridge DC/DC Converters in a Power Electronic Traction Transformer", IEEE Transactions on Power Electronics, Vol. 33, No. 2, pp.1696-1714, February-2018.
[15]. Anping Tong, et.al, "Modeling and Analysis of a Dual-Active-Bridge-Isolated Bidirectional DC/DC Converter to Minimize RMS Current with whole Operating Range", IEEE Transactions on Power Electronics, Vol. 33, No. 6, pp. 5302-5316, June-2018.
[16]. Kazuto Takagi, et.al, "Dynamic Control and Performance of a Dual-Active-Bridge DC–DC Converter", IEEE Transactions on Power Electronics, Vol. 33, No. 9, pp.7858-7866, September-2018.
[17]. Shuai Shao, et.al, "Optimal Phase-Shift Control to Minimize Reactive Power for a Dual Active Bridge DC–DC Converter", IEEE Transactions on Power Electronics, Vol. 34, No. 10,pp.10193-10205, October-2019.
[18]. M. A. Awal, et. al., "Capacitor Voltage Balancing for Neutral Point Clamped Dual Active Bridge Converters", IEEE Transactions on Power Electronics, Vol. 35, No. 10, pp. 11267-11276, October-2020.
[19]. V. Narasimhulu, D. V. Ashok Kumar, and Ch. Sai Babu, "Recital analysis of multilevel cascade H-bridge based active power filter under load variation," SN Applied Sciences, Nov. 2019, vol. 1, no. 12, Art. No. 1621. DOI: https://doi.org/10.1007/s42452-019-1669-8.
[20]. Simone Pistollato, et. al., "A Low Complexity Algorithm for Efficiency Optimization of Dual Active Bridge Converters", IEEE open Journal of Power Electronics, Volume 2, 2021, pp.18-32.
[21]. Wenguang Zhao, et. al., "Improved Model-Based Phase-Shift Control for Fast Dynamic Response of Dual-Active-Bridge DC/DC Converters", IEEE Journal of Emerging and Selected Topics in Power Electronics, Vol. 9, No. 1, pp.223-231, February-2021.
[22]. Ioannis Mandourarakis; Vasiliki Gogolou; Eftichios Koutroulis; Stylianos Siskos, Integrated Maximum Power Point Tracking System for Photovoltaic Energy Harvesting Applications, IEEE Transactions on Power Electronics, vol.37, no. 8, pp. 9865 - 9875, August 2022.
[23]. G. Jhansi Rani**,** P. Srinivas, "Implementation of Dual Active Full Bridge DC-DC Converter Using Phase Shift Control Technique" International Journal of Creative Research Thoughts, Volume 6: Issue: 2 April 2018, ISSN: 2320-2882, DOI: http://doi.one/10.1729/Journal.35793.
[24]. G. Jhansi Rani. E. Vidyasagar, "Control of PV Integrated DAB Under Shading Conditions Using Improved Incremental Conductance MPPT Scheme" Journal of Harbin Engineering University, Volume 44, Issue 11, pages: 644-650, NOV-2023. ISSN: 1006-7043.
[25]. B. Anil Kumar and G. Jhansi Rani, "Design and Performance Analysis of Battery Electric Vehicle using MATLAB/Simulink," Journal Of Technology, ISSN 1012-3407 vol. 14, no. 3, 2024.
[26]. B. Anil Kumar and G. Jhansi Rani "Design and Comparative analysis of Analysis of Battery Electric Vehicle" Journal of Engineering and Technology Management, ISSN 1879-1719. vol 73 2024.